

Oil Spill GF-1 Remote Sensing Image Segmentation Using an Evolutionary Feedforward Neural Network

Jianchao Fan, Dongzhi Zhao, and Jun Wang

Abstract—To improve self-made satellites in the marine oil spill monitoring accuracy, it is presented that a Gao Fen (GF-1) satellite marine oil spill remote sensing (RS) image classification algorithm based on a novel evolutionary neural network. First, a non-negative matrix factorization (NMF) algorithm is employed to extract the image features. Compared with basic features, such as the image spectrum and texture, structuring more targeted oil spill image localization non-negative character fits better for the physical significance of remote sensing images. Furthermore, on the basis of the new features, a new feedforward neural network structure with particle swarm optimization (PSO) algorithm is proposed for GF-1 RS image segmentation. Simulation results of the oil spill event substantiate the effectiveness of the proposed approach to GF-1 satellite image segmentation.

I. INTRODUCTION

WITH the increasing human activities in the oceans, shipping and offshore oil have serious impacts on the marine environment, and even to be a fundamental change. This not only brings direct harm to the marine life, but also takes indirectly harm to the social, economic and human health along the coast [1]. Because there is a huge uncertainty in the natural marine environment, and coupled with the objective conditions of shipping and oil platform, oil spill disasters are inevitable [2]. Therefore, it is very necessary to perform fast and accurate monitoring of marine oil spill.

Compared with traditional on-site oil spill monitoring, the use of remote sensing technology has the macroscopic characteristics, which could quickly and accurately find an oil spill area [3]. Currently, the detection approach of monitoring the phenomenon of marine oil spill are usually divided into two types, which are optical and synthetic aperture radar (SAR) remote sensing images. Among all satellite sensors, SAR is still the most utilized for operational oil spill detection [4]. The discrimination of oil spills and look-alike phenomena (e.g., low wind area, wind front area and natural slicks) on SAR is a crucial task in marine oil spill

J. Fan and J. Wang are with the School of Control Science and Engineering, Dalian University of Technology, Dalian, Liaoning, China (email: jcfan@nmemc.gov.cn, jwang@mae.cuhk.edu.hk). J. Fan and D. Zhao are with the Department of Ocean Remote Sensing, National Marine Environmental Monitoring Center, Dalian, Liaoning, China (email: dzzhao@nmemc.gov.cn). J. Wang is also with the Department of Mechanical and Automation Engineering, The Chinese University of Hong Kong, Shatin, New Territories, Hong Kong.

This research was supported by the project (201305003) "Beidaihe Adjacent Waters Typical Ecological Disasters and Pollution Monitoring Key Technologies Integrated Applications", and also supported by the Foundation (201313) of Key Laboratory of Marine Spill Oil Identification and Damage Assessment Technology. The work described in the chapter was also supported by the Research Grants Council of the Hong Kong Special Administrative Region, China, under Grants CUHK416812E.

detection. In order to make the best use of the large variety of statistical and machine learning classification methods, Xu et al. assessed their performance differences and make recommendations for classifier selection and improvement in RADARSAT-1 imagery [5]. Migliaccio *et al.* [6] adopted fully polarimetric SAR data to observe marine oil spill detection in the black areas of the image through the polarization constant false alarm rate. After that the target decomposition theory is employed to obtain the oil spill area. However, its spatial and temporal coverage and its high costs limit the application capability.

Optical satellite remote sensing data with much intuitive and rich band information, has been widely used in marine oil spill information extraction. The modern generation of visible sensors offer possibilities for global environmental monitoring and land-cover mapping at high-resolution scale using multi-polarization data [7]. At the beginning, Hu *et al.* [8] commonly used MODIS data for monitoring oil spill areas. They carried out dynamic analysis and judgment of spread tendency. However, the lower spatial resolution of MODIS data for accurate determination of the scope of oil spills have some weakness [9]. With the advent of self-made GF-1 satellite data, the visible satellite RS data has been widely applied in the field of water quality monitoring and land cover survey. After the GF-1 satellite was successfully launched on April 26, 2013, it could provide high-precision, wide range of space observation services. Thus, it also provides a opportunity for oil spill monitoring. There is now an increasing volume of RS data due to high spatial resolution and high time resolution [10]. Thus, automated image segmentation and classification methods are desired to replace manual interpretation, which is subjective and labor intensive [11]. Image segmentation is regarded as a process of partitioning digital images into multiple regions or objects. These objects provide more information than individual pixels since the interpretation of images based on objects is more meaningful than the interpretation based on individual pixel only [12]. Image segmentation is considered as an important task in the analysis, interpretation, and understanding of images and is also widely used for image processing purposes such as classification and object recognition [13]. Singha *et al.* [14] described the development of a new approach to oil spill detection by employing two different artificial neural networks (ANN), used in sequence. Ganta *et al.* [15] represented a method for segmenting oil spill regions in satellite images taken in broad daylight using illumination-reflectance based level set model. However, different types of oil-water mixture under different spectral

response characteristics of seawater background, which is completely different. If monitoring relies on the spectral and texture characteristics of the image, it will lose much useful information. How to find the best features for RS image segmentation is a new challenge. In addition, in the actual RS segmentation problem, there are commonly huge data. If the basic neural network structure is adopted, the computation is very complex. So how to construct a simple structure and converge quickly is very necessary.

The remainder of this paper is organized as follows. Section II presents the modified non-negative matrix factorization algorithm. The novel neural network structure with particle swarm optimization is presented in section III. Section IV highlights the potential of the proposed approach through experimental examples. Concluding remarks are presented in Section V.

II. MODIFIED NON-NEGATIVE MATRIX FACTORIZATION

Analysis on separate matrices or slices extracted from a data block often faces the risk of losing the covariance information among various mode. To discover hidden components within the data, the analysis tools should be adopted to reflect the multidimensional structure of the data [16]. Non-negative matrix factorization (NMF) algorithm is first proposed by Lee and Seung [17]. NMF is distinguished from the other methods, such as principal component analysis (PCA), by its use of non-negativity constraints, which has more realistic application characteristics with real physical significance. Furthermore, more newly constructive images are localized features that correspond to better intuitive notions in PolSAR images.

Let $V_{n \times m}$ denote each single polarimetric SAR image data S_{hh}, S_{hv}, S_{vh} and S_{vv} , where n is the number of pixels, m is the number of basic feature in the original image. The matrix factorization is expressed as follows,

$$V \approx WH \quad (1)$$

where $W_{n \times r}$ is the basis matrix, $H_{r \times m}$ is the corresponding coefficient matrix, r is the feature dimension after factorization. Each column vector of V is approximately equals to the linear combination of the matrix W , and H is the combination coefficient.

In order to perform non-negative matrix factorization, Eqn. (1) can be defined as a constrained optimization problem as follows:

$$\begin{aligned} \min \quad & f(W, H) \\ \text{s.t.} \quad & W \geq 0, H \geq 0 \end{aligned} \quad (2)$$

where $f(W, H)$ is an objective function, which characterizes the degree after decomposition similar to the original remote sensing data matrix. The constraints ensure the nonnegativity. Considering the noises of PolSAR remote sensing images, an alternative objective function is built as,

$$f(W, H) = \sum_{i=1}^n \sum_{j=1}^m (V_{ij} - (WH)_{ij})^2. \quad (3)$$

In order to obtain the best solution to this constraint optimization problem, we modify the original NMF algorithm and perform alternatively minimization (3). When one vector is computed, the other vectors are fixed. Thus, the stationary points can be estimated via the following updating rules:

$$H_{kj} \leftarrow \max\{0, H_{kj} \frac{(W^T V)_{kj}}{(W^T W H)_{kj}}\} \quad (4)$$

$$W_{ik} \leftarrow \max\{0, W_{ik} \frac{(V H^T)_{ik}}{(W H H^T)_{ik}}\} \quad (5)$$

where $k = 1, \dots, r$. Rules (4) and (5) are referred as the modified non-negative factorization (MNMF). Each feature extraction method for matrix factorization factor W and H imposes different constraints limiting conditions. In the PCA algorithm, the matrix W is imposed column vectors on the orthogonal constraint. Although the direction of the extracted characteristic has a large variance of statistical significance, that wherein the linear combination of positive and negative is not visually apparent on the understanding. MNMF algorithm matrix decomposition process, due to the non-negative constraints, there is no redundancy negative features generated.

III. THE EVOLUTIONARY FEEDFORWARD NEURAL NETWORK

A multi-input, single-output feedforward neural network is chosen as an example to illustrate proposed an evolutionary feedforward neural network (EFNN) as shown in Fig. 1. There is only one connection between two neurons in adjacent layers. The delay dynamic operators $z^{-\tau_{ji}^{(1)}}$ and $z^{-\tau_{pq}^{(2)}}$ are associated in the first hidden layer and input layer, the last hidden layer and output one, respectively. These two dynamic parameters are together adaptive adjusted with the connection weights ω and the threshold b .

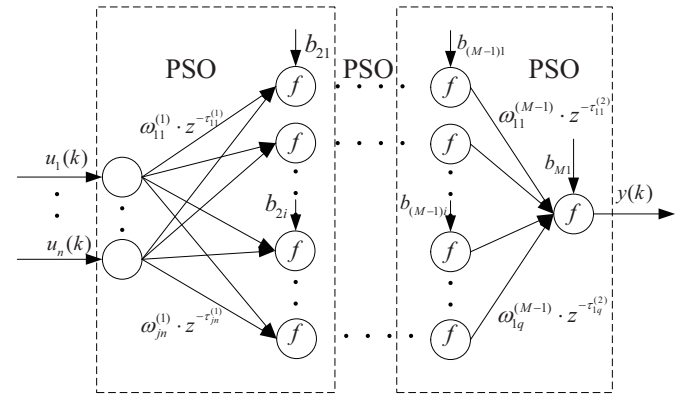


Fig. 1. The structure of the proposed evolutionary feedforward neural network

In the hidden layers, the input and output relationships can be expressed as (6) and (7), respectively

$$net_j^{(l)}(k) = \sum_{i=1}^{N^{(l-1)}} \omega_{ji}^{(l-1)} O_i^{(l-1)}(k) + b_{ij} \quad (6)$$

$$O_j^{(l)}(k) = f[net_j^{(l)}(k)] \quad (7)$$

where $net_j^{(l)}(k)$ and $O_j^{(l)}(k)$ denote the input and output of the j th neural in the l th layer at time k , respectively. The weight connecting the j th neuron in the l th layer to the i th neuron in the $(l-1)$ th layer are represented by $\omega_{ji}^{(l-1)}$. It is noted that j changes from 1 to N^l , i changes from 1 to N^{l-1} . b_{lj} denotes the threshold parameter of the j th neural in the l th layer. $f[\cdot]$ is a nonlinear activation function, written as

$$f(x) = K \frac{1 - e^{-cx}}{1 + e^{-cx}} \quad (8)$$

Joined the dynamic delay operators among the connections, the description of the first hidden nodes and output neurons can be expressed respectively as

$$net_j^{(2)}(k) = \sum_{i=1}^{N^{(1)}} \omega_{ji}^{(1)} O_i^{(1)}(k - \tau_{ji}^{(1)}) + b_{2j} \quad (9)$$

$$net_p^{(M)}(k) = \sum_{q=1}^{N^{(M-1)}} \omega_{pq}^{(M-1)} O_q^{(M-1)}(k - \tau_{pq}^{(2)}) + b_{Mq} \quad (10)$$

here $\tau_{ji}^{(1)}$ and $\tau_{pq}^{(2)}$ denote the associated delay connecting the hidden layers with input and output layers, respectively. The parameters $\tau_{ji}^{(1)}$ and $\tau_{pq}^{(2)}$ are adaptively adjusted by PSO algorithm until reaching the minimum value of fitness function, and changing from 0 to τ_{\max} . As a result, each connection between the neurons can be seen on a random time delay $\tau_{ji}^{(1)}$ so that the network has the time sequence. The current moment output may be related to a few moments of inputs, which enhances the dynamic character of EFNN. The dynamic delays between the first hidden one and input layer fully express a causal relationship between input and output. That mainly focuses on nonlinear characters.

The parameters of EFNN are optimized using the PSO algorithm, which mimics the behavior of a swarm of insects or a school of fish. If one of the particles discovers a good path to food, the rest of the swarm will be able to follow instantly even if they are far away in the swarm. Swarm behavior is modeled by particles in multidimensional space and have two characteristics: position and velocity. These particles wander around the hyperspace and remember the best position they have discovered. They communicate good positions to each other and adjust their own position and velocity [18]. There are four main parameters in the PSO algorithm, which are specified as follows. The location of the i th particle is represented as $x_i = \{x_{i1}, x_{i2}, \dots, x_{iD}\}$, where $x_{id} \in [x_{\min,d}, x_{\max,d}]$, $d = 1, \dots, D$. $x_{\min,d}$ and $x_{\max,d}$ are the lower and upper bounds for the dimension d , respectively. The best previous position P_{best} of the i th particle is denoted as $p_i = (p_{i1}, p_{i2}, \dots, p_{iD})$. Let $v_i = (v_{i1}, v_{i2}, \dots, v_{iD})$ be the current velocity, which is limited to a maximum velocity $V_{\max} = (v_{\max,1}, \dots, v_{\max,D})$. The position p_{gbest} of the best one among all the particles in the population is represented as $p_g = (p_{g1}, p_{g2}, \dots, p_{gD})$. The velocity and position of each particle are updated toward its P_{best} and p_{gbest} locations according to (11)

$$\begin{cases} v_{id}(k+1) = wv_{id}(k) + c_1 rand_{1d}[p_{id}(k) - x_{id}(k)] \\ \quad + c_2 rand_{2d}[p_{gd}(k) - x_{id}(k)] \\ x_{id}(k+1) = x_{id}(k) + v_{id}(k+1) \end{cases} \quad (11)$$

where $w \in [0, 1]$ is the inertia weight, determining how much of the previous velocity of the particle is preserved. And $rand_1, rand_2 \in [0, 1]$ denote two uniform random numbers, c_1, c_2 are acceleration constants. In (11), the first term is the movement of particles on the current self-confidence, and is related to their speed and inertia weight; the second term represents a "cognitive" process, which is the movement of particles from some of their own experience; the third term is the social part, which represents the cooperation among the individuals. The updating position of each particle is made up of these three terms as shown in Fig. 2

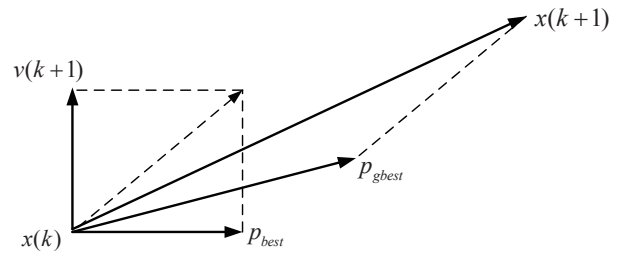


Fig. 2. The vector diagram of the particle velocity

In order to overcome the drawback of trapping into the local optima points, a wavelet-theory-based mutation operation is added in the optimization process. It applied the wavelet theory to enhance the PSO in exploring the solution space more effectively for a better solution as (12)

$$\vec{x}_j(k) = \begin{cases} \vec{x}_j(k) + \sigma(\vec{x}_{\max} - \vec{x}_j(k)) & \text{if } \sigma > 0 \\ \vec{x}_j(k) + \sigma(\vec{x}_j(k) - \vec{x}_{\min}) & \text{if } \sigma < 0 \end{cases} \quad (12)$$

where σ was dependent on the wavelet function curve. This method could make great effect on the search space dynamic adjustment, which attempts to promote convergence, discovery, and improve solutions.

IV. SIMULATION RESULTS

In order to substantiate the effectiveness of proposed model for GF-1 RS image segmentation, the pipeline explosion event happened at November 22, 2013 was adopted for analysis. GF-1 satellite has four bands with the spatial resolution 2m/8m/16m. In the course of this event in track, the 16m GF-1 image with width 250Km at Nov. 22, 2013 is employed. The scene of that explosion day is shown in Fig. 3. It is seen that a cloud of black billowing smoke blew over the city. After that, it is found that there are some oil spill areas from GF-1 satellite image on Nov. 26, 2013. The special oil spill area is cut as shown in Fig. 4. There are four main objectives in the image, whose spectral values are shown in Fig. 5.

There are some basic distinctions from the spectral view. However, the oil and sea water is very similar. So, MNMF



Fig. 3. The GF-1 image at Nov. 22, 2013

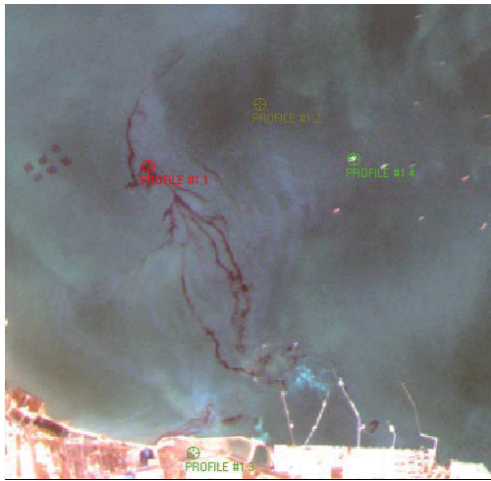


Fig. 4. The cut image of oil spill area

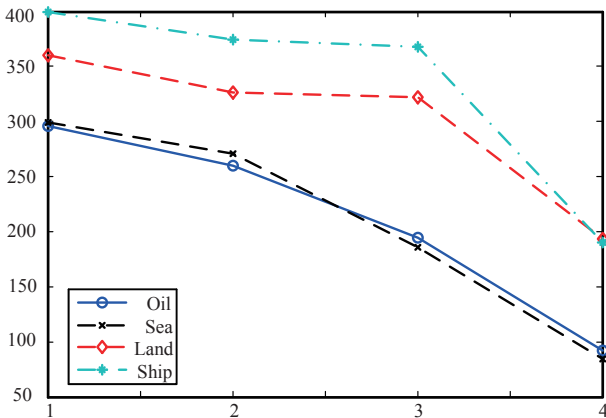


Fig. 5. The spectral values of different objectives

is adopted to extract the features of this GF-1 image. The input vectors are constructed, and then dealt by using EFNN. The segmentation result is shown in Fig. 6. It is seen that the proposed approach can obtain good segmentation results. However, some dark areas in the sea are confused into the oil spill area. In order to compared with other algorithms, the index of overall accuracy and Kappa coefficient are introduced to evaluate as below:

$$O = \frac{\text{the number of correctly segmentation samples}}{\text{the total number of samples}} \quad (13)$$

More over, a discrete multivariate analysis technique is used to test whether the overall agreement in the different separate error matrices is significantly different. The measure of agreement called Kappa coefficient [19] is adopted to assess the significant differences, which is defined as follows:

$$\kappa = \frac{N \sum_{k=1}^C N_{kk} - \sum_{k=1}^C N_{k+} N_{+k}}{N^2 - \sum_{k=1}^C N_{k+} N_{+k}} \quad (14)$$

where N is the number of all samples, C is the number of clusters, N_{kk} denotes the number of correctly classified. N_{k+} and N_{+k} indicate, respectively, the number for class i and the number of clustering to class i .

The overall accuracy and Kappa coefficient are tabulated in Table I. A classic feedforward neural network, such as the BP neural network, is added in the simulation. According to the results, MNMF+EFNN algorithm outperforms other ones. The MNMF method could obtain the best features. And then these are input into the EFNN for GF-1 image segmentation.

TABLE I
CLUSTERING PERFORMANCE OF SIX ALGORITHMS ON POLSAR IMAGE SEGMENTATION

	Overall Accuracy	κ coefficient
FNN	74.12%	0.7292
EFNN	81.56%	0.7834
MNMF+EFNN	87.41%	0.8629

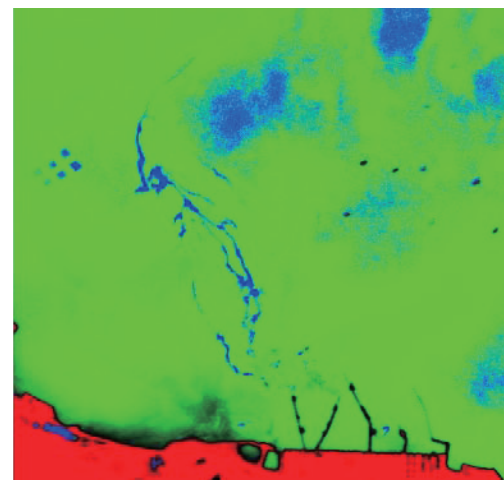


Fig. 6. The GF-1 image segmentation result

V. CONCLUSIONS

A novel MNMF+EFNN model is developed for GF-1 oil spill RS image segmentation, which effectively extracts the target feature information and classifies the oil spill area. Through the oil spill event, its validity for oil spill monitoring is demonstrated.

REFERENCES

- [1] C. Brekke and A. H. S. Solberg, "Oil spill detection by satellite remote sensing," *Remote Sensing of Environment*, vol. 95, pp. 1–13, 2005.
- [2] S. Singha, M. Vespe, and O. Trieschmann, "Automatic synthetic aperture radar based oil spill detection and performance estimation via a semi-automatic operational service benchmark," *Marine Pollution Bulletin*, vol. 73, no. 1, pp. 199–209, 2013.
- [3] B. Tansel, "Propagation of impacts after oil spills at sea: Categorization and quantification of local vs regional and immediate vs delayed impacts," *International Journal of Disaster Risk Reduction*, vol. 7, pp. 1–8, 2014.
- [4] M. Migliaccio, A. Gambardella, F. Nunziata, M. Shimada, O. I. Lee, and J. Y. Jung, "The PALSAR polarimetric mode for sea oil slick observation," *IEEE Transactions on Geoscience and Remote Sensing*, vol. 47, no. 12, pp. 4032–4041, 2009.
- [5] L. L. Xu, J. Li, and A. Brenning, "A comparative study of different classification techniques for marine oil spill identification using radarsat-1 imagery," *Remote Sensing of Environment*, vol. 141, pp. 14–23, 2014.
- [6] M. Migliaccio, A. Gambardella, and M. Tranfaglia, "SAR polarimetry to observe oil spills," *IEEE Transactions on Geoscience and Remote Sensing*, vol. 45, no. 2, pp. 506–511, 2007.
- [7] O. Antropov, Y. Rauste, A. Lonnqvist, and T. Hame, "PolSAR mosaic normalization for improved land-cover mapping," *IEEE Geoscience and Remote Sensing Letters*, vol. 9, no. 6, pp. 1074–1078, 2012.
- [8] C. M. Hu, X. F. Li, W. G. Pichel, and K. F. E. Muller, "Detection of natural oil slicks in the NW gulf of mexico using modis imagery," *Geophysical Research Letters*, vol. 36, no. 1, pp. L01 604, 1–5, 2009.
- [9] B. Bulgarelli and S. Djavidnia, "On MODIS retrieval of oil spill spectral properties in the marine environment," *IEEE Geoscience and Remote Sensing Letters*, vol. 9, no. 3, pp. 398–402, 2012.
- [10] M. Lee and J. Y. Jung, "Risk assessment and national measure plan for oil and HNS spill accidents near korea," *Marine Pollution Bulletin*, vol. 73, no. 1, pp. 339–344, 2013.
- [11] A. Frery, R. Cintra, and A. Nascimento, "Entropy-based statistical analysis of PolSAR data," *IEEE Transactions on Geoscience and Remote Sensing*, vol. 51, no. 6, pp. 3733–3743, 2013.
- [12] J. C. Fan, M. Han, and J. Wang, "Single point iterative weighted fuzzy c-means clustering algorithm for remote sensing image segmentation," *Pattern Recognition*, vol. 42, no. 11, pp. 2527–2540, 2009.
- [13] P. Ghamisi, M. S. Couceiro, J. A. Benediktsson, and N. M. F. Ferreira, "An efficient method for segmentation of images based on fractional calculus and natural selection," *Expert System and Application*, vol. 39, no. 16, pp. 12 407–12 417, Nov. 2012.
- [14] S. Singha, T. J. Bellerby, and O. Trieschmann, "Satellite oil spill detection using artificial neural networks," *IEEE Journal of Selected Topics in Applied Earth Observations and Remote Sensing*, vol. 6, no. 6, pp. 2355–2363, 2013.
- [15] R. Ganta, S. Zaheeruddin, N. Baddiri, and R. Rao, "Segmentation of oil spill images with illumination-reflectance based adaptive level set model," *IEEE Journal of Selected Topics in Applied Earth Observations and Remote Sensing*, vol. 5, no. 5, pp. 1394–1402, 2012.
- [16] A. Cichocki, R. Zdunek, A. H. Phan, and S. Amari, *Nonnegative Matrix and Tensor Factorizations: Application to Exploratory Multi-way Data Analysis and Blind source Separation*. Chichester: Wiley, 2009.
- [17] D. D. Lee and H. Seung, "Learning the parts of objects by non-negative matrix factorization," *Nature*, vol. 401, pp. 840–850, 1999.
- [18] J. Kennedy and R. Eberhart, "Particle swarm optimization," in *Proc. of IEEE International Conference on Neural Networks*, 1995, pp. 1942–1948.
- [19] W. B. Tao, H. Jin, and Y. M. Zhang, "Color image segmentation based on mean shift and normalized cuts," *IEEE Transactions on Systems, Man and Cybernetics, Part B: Cybernetics*, vol. 37, no. 5, pp. 1382–1389, 2007.